Ma *et al. J Wireless Com Network* (2023) 2023:30
https://doi.org/10.1186/s13638-023-02238-3

EURASIP Journal on Wireless Communications and Networking

RESEARCH Open Access

A monopole broadband circularly polarized antenna with coupled disc and folded microstrip stub lines

Zhonghua Ma[1], Jiaxiang Chen[1], Chen Li[1] and Yanfeng Jiang[2*]

*Correspondence:
jiangyf@jiangnan.edu.cn

[1] School of Marine Information Engineering, Jimei University, Xiamen 361021, Fujian, China
[2] College of IoT Engineering, Jiangnan University, Wuxi 214122, China

Abstract

A broadband circularly polarized (CP) printed monopole antenna which fed by coplanar waveguide (CPW) is proposed in the paper. The structure of the novel antenna includes a quarter circular disc radiating monopole, a coupled circular patch, and a bent L-shaped microstrip stub line. The L-shaped microstrip stub line is used to widen the impedance bandwidth and generate a horizontal component of the electromagnetic wave. The adoption of the asymmetric ground coplanar waveguide structure with the single-feed technology and the coupled circular patch, simultaneously achieve wide impedance bandwidth and wide axial ratio (AR) bandwidth. The structure parameters and the surface current of the designed antenna are analysed. The simulation and the measurement are conducted, showing good characterizations of the designed antenna. The 10-dB impedance bandwidth is 7.57 GHz, the fractional bandwidth from 6.05 to 13.62 GHz is 76.9%, the 3-dB axial ratio bandwidth is 3.01 GHz, and the fractional bandwidth from 6.05 to 9.06 GHz is 39.8%. The antenna can generate right/left hand circularly polarized waves in the direction of ±z axis. The designed antenna has wide applications in the fields of Internet of Things (IoT), broadband dual-CP communication systems and polarization diversity systems, wireless personal area network and other advanced communication systems.

Keywords: Circularly polarized (CP), Axial ratio (AR), Coplanar waveguide (CPW), L-shaped microstrip stub, Dual-CP

1 Introduction

In recent years, circularly polarization (CP) antennas have been attracted extensive attention in wireless systems such as navigation, radar, satellite and radio-frequency identification (RFID) because of its flexibility in the orientation angle between transmitter and receiver, its better mobility and weather penetration, and less multipath reflection [1–3]. Circular polarization can generally be achieved by exciting two orthogonal modes with equal amplitude but 90° phase difference.

Planar printed antenna has the advantages of low cost, easily manufacture and low profile, which is often used in the design of CP antenna [4]. CPW feed has small dispersion and low radiation loss, and its working frequency can reach millimeter wave band.

In the CPW fed microstrip antenna, the active devices can be integrated much easier, with series and shunt connection on one side of the substrate, avoiding the via-connection in the substrate [5].

In order to achieve both wide impedance bandwidth and wide axial ratio (AR) bandwidth with single antenna, wideband circularly polarized antenna was proposed by trimming the feed structure and the loading slots. J. W. Wu et al. proposed an asymmetric feeding monopole rectangular radiation patch in 2010, with embedded slits and stubs on the deformed ground to achieve 31.6% AR bandwidth and 102.5% impedance bandwidth [6]. Zhang et al. proposed a CPW fed planar printed monopole antenna with broadband CP characteristics in 2013. The proposed antenna consists of a rectangular patch and an improved ground plane. The AR and the impedance bandwidth are enhanced by adding vertical stub and cutting horizontal slot [7]. It shows that the antenna can achieve wide impedance bandwidth and wide AR bandwidth at the same time, with the 3-dB AR bandwidth reaching 44.9% and the 10 dB impedance bandwidth reaching 76.9%. The broadband CP monopole antennas in [8–10] mainly utilized complex patch structures or embedded slots & stubs ground planes. Ref. [11] reported the coupling effect between a monopole antenna and a short sleeve for the excitation of both the monopole and the traveling wave resonant modes. However, the corresponding 3-dB AR bandwidth is only 5%.

It is worth noting that special slot antennas fed by CPW structures, such as the staircase-shaped slot adopted in [12] and the regular-hexagonal structure adopted in [13], also exhibit the broadband CP performance. Ref. [14] proposed a CPW-fed 3D MIMO ground-radiating cubic antenna (CA) for biotelemetry, which achieves CP radiation in two bands of 2.45 GHz and 5.8 GHz. However, with the large size of the antenna, it is difficult to conform it to the other communication devices. The CP antenna reported in Ref [15] is composed of three asymmetrical rectangular slots. The axial ratio bandwidth can reach 2.3 GHz. The 3-dB axial ratio bandwidth overlaps with the 10-dB impedance bandwidth very well. Its working frequency spectrum can cover the bands of RFID, WLAN and WiMAX. Ref. [16] proposed an ultra-wideband (UWB) CP antenna with continuous phase feeding. Its 3-dB AR bandwidth reaches 133.3%, but the feeding network is very complex with the large antenna size. Ref. [17] performed CPW feeding for the first time on a quasi-magnetic dipole (PQMD), in which the planar quasi-magnetic dipole as well as the printed electric dipole work together to achieve the circular polarization performance with the extreme narrow working bandwidth. Ref. [18] uses dual port feedings to achieve double circular polarization modes for the port isolation, while the antenna proposed in this paper only needs one port to achieve right/left circular polarization in the $\pm$z axis direction at the same time. Ref. [19] adopts coplanar waveguide feed to excite quadrilateral-shaped monopole antenna, which shows excellent CP performance with small size. An array element in antenna is proposed in the paper. Ref. [20] proposed a monopole antenna fed by a square coplanar waveguide surrounding the antenna. The impedance bandwidth is 12 GHz, but the AR bandwidth is relatively narrow. In addition, wavelet analysis can be used to design fractal geometry. When fractal structure is used for antenna design, a tortuous and complex current path can be constructed. The current distribution on the antenna has a certain level and self-similarity, so it can produce multi-frequency radiation characteristics. When multiple frequencies

on the antenna are close to each other, broadband operation can be realized [21–28]. However, the design of fractal circularly polarized antenna is relatively difficult and can't be used practically until now. Above all, it is still a challenge for the optimization of the monopole antenna with both wide AR bandwidth and wide impedance bandwidth.

In the paper, a novel CPW-fed quarter-circular monopole antenna with asymmetric ground plane and bent L-shaped stub line loading is designed to achieve wide impedance matching and broadband CP operating bandwidth. The CP radiation is implemented on the quarter-circle microstrip patch monopole using an asymmetric ground plane. To expand the impedance bandwidth and the AR bandwidth, a bent L-shaped stub line is assembled on the left of the monopole, and a circular patch is coupled above the monopole. The measurements show that the impedance bandwidth is 76.9%, and the 3-dB AR bandwidth is 39.8%. At the same time, the size of the antenna is relatively small, with the low profile and the simple feeding structure.

2 Method

2.1 Antenna design

Figure 1 shows the schematic structure of the designed wideband circularly polarized antenna. The antenna is implemented on Kappa 438 substrate, with a relative dielectric constant of 4.38, a loss tangent of 0.005 and a thickness of 1.016 mm. There is no ground on the back of the antenna base plate. The area is 24.5 mm × 25 mm. The antenna is fed by coplanar waveguide, excited by 50 Ω microstrip with width W_f. The microstrip line with length l_n realizes the impedance transformation of the antenna and the feed line. The grounds of the microstrip are located on both sides of the feeder with a spacing of g. The ground of the antenna is designed based on the asymmetric structures with different sizes. The designed antenna is simulated by ANSYS High Frequency Structure Simulator (HFSS). Table 1 shows the final optimization parameters of the proposed antenna.

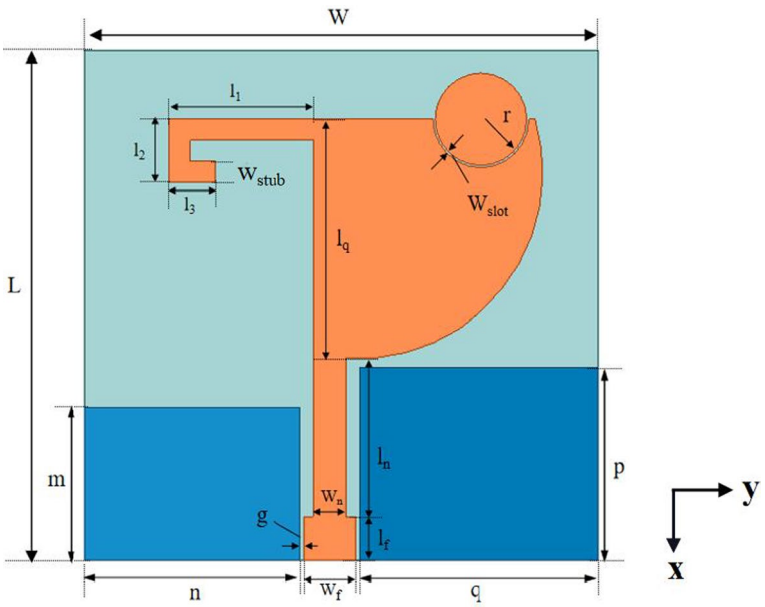

Fig. 1 Top view of the designed circular polarization antenna structure

Table 1 Key parameters of the proposed antenna (unit: mm)

W	L	l_1	l_2	l_3	l_f	l_n	l_q	r
24.5	24	6.9	2	2.2	2.05	7.5	11.25	2
W_f	W_n	W_{slot}	p	q	m	n	W_{stub}	g
2.45	1.55	0.1	9.1	11.37	7.2	10.27	0.5	0.2

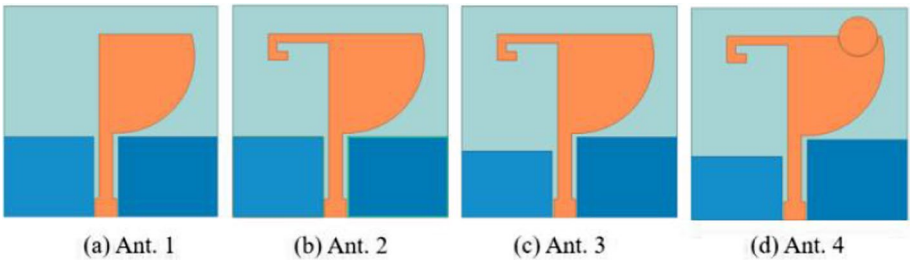

Fig. 2 The schematic structures of the four evolutions during the design process. **a** Ant. 1. **b** Ant. 2. **c** Ant. 3. **d** Ant. 4. Ant.4 is the accomplished antenna in the paper

The design process includes the four iterative evolution steps, as shown in Fig. 2. Their corresponding reflection coefficients and AR results are shown in Fig. 3. The length l_q of the basic monopole antenna is quarter-wavelength at frequency of 7.5 GHz, as expressed in Eq. (1):

$$l_q = \frac{\lambda_g}{4} = \frac{c}{4 \times f_{res}} \tag{1}$$

in which λ_g the wavelength of the corresponding frequency, f_{res} the frequency parameter.

In the first step, as shown in Fig. 2a, the first generation Ant.1 is a simple CPW fed quarter circular monopole patch antenna. Figure 3a shows that the reflection characteristic of Ant.1 at high frequency is poor. Although the circular polarization can be synthesized by two mutually orthogonal electromagnetic wave components, the radiation of Ant.1 in the horizontal direction is weak. In order to introduce a horizontal component, at the second step, a bent L-shaped stub is loaded on the quarter circular radiation patch, as shown Ant.2 in Fig. 2b. Figure 3b exhibits that its AR decreases obviously, while its CP characteristics are improved significantly. The bent L-shaped microstrip stub line introduces a resonance point between the 10 GHz and 11 GHz frequency band to broaden the impedance bandwidth.

The AR curve in Fig. 3 is the evolution process from the first-generation antenna in Fig. 2a to the final ones in Fig. 2d. During this trial and error evolution process, it can be seen that the current distribution and current flow direction are changed mainly by adding structures. The AR value is reduced during the evolution process, from 10 dB at the beginning to less than 3 dB. An asymmetric ground plane and an asymmetric feeding of the monopole are designed in Ant. 3 (as shown in Fig. 2c). This asymmetric ground feeding structure can generate additional horizontal component of electromagnetic waves, which can be combined with the horizontal components by L-shaped stub and

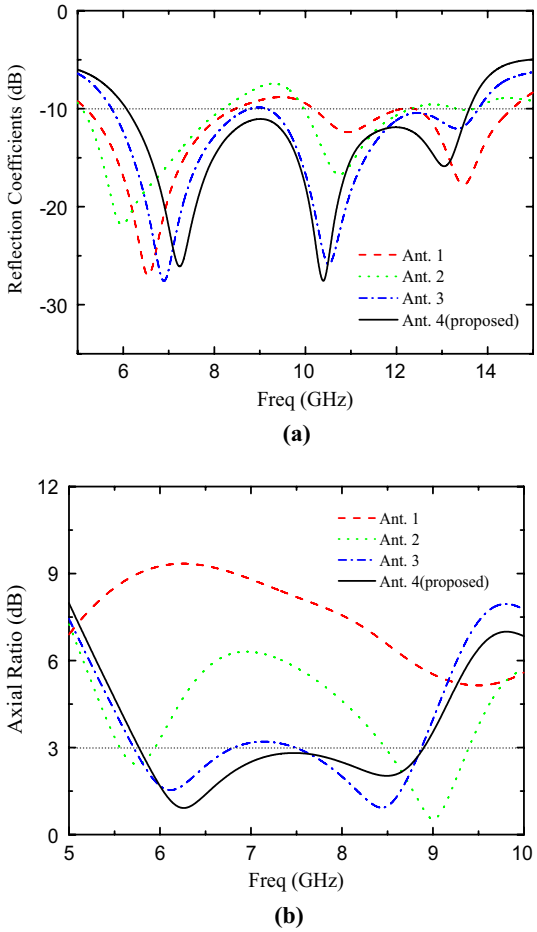

Fig. 3 Performance comparison of the four designed antennas. **a** The relationship between the frequency and the reflection coefficient. **b** The relationship between the frequency and the axial ratio (AR)

the vertical electromagnetic wave components on monopoles. The combination can be useful to generate the circularly polarized wave in the far field. The surface horizontal current on the stub is expressed as [29]:

$$\vec{J} = \vec{y}\frac{Ae^{-j\beta y} + Be^{-j\beta y}}{W_{stub}}\cos\left(\frac{\pi\left(y - y_{st}\right)}{l_1}\right)\delta(z-d) \tag{2}$$

where A and B are the coefficients for the incident and reflected waves, respectively, and β the propagation constant of the stub, y_{st} the coordinates of the center point on the stub, $l_1$and W_{stub} the length and width, respectively, of the stub.

HFSS software is used to simulate and optimize the length and width of the stub, as well as the size of the asymmetric ground to change the current distribution of the antenna, thereby increasing the axial ratio bandwidth.

Finally, Ant.4 is designed, in which a circular disk is coupled to the monopole patch to introduce the perturbation, as shown in Fig. 2d. Figure 3d shows the reflection characteristic and the AR of Ant.4. The excitation of the circular patch is provided by the monopole through the coupling slot W_{slot} to increase the AR bandwidth, as shown in

Fig. 4. The radius r of the disk has the following relationship with the radius l_q of the quarter monopole [30].

$$r \approx \sqrt{\frac{l_q}{\pi}} \tag{3}$$

Figure 4 shows the surface current distributions of Ant.4, with 6.5 GHz in Fig. 4(a) and 8.5 GHz in Fig. 4b. It clearly shows that the CP is mainly generated by the rotating current components on the quarter-circle radiating monopole. As shown in the + z direction, the surface current rotates counterclockwise, which leads to the radiation of RHCP. The circular polarization characteristic of the narrow-band circular antenna at the ends of the low frequency and the high frequency can be realized by folding the microstrip stub line and asymmetric ground, with additional two resonant modes with the axial ratio below 3 dB appear, with 6.5 GHz and 8.5 GHz as centre frequencies, respectively. The difference in the structure of the ground on both sides of the feeder leads to the stronger current in the vertical direction on the left side, while right side with concentrated current in the horizontal direction. The currents of the two asymmetrical grounds are orthogonal to each other, leading to broadband range for the circular polarization.

3 Discussion

3.1 Parameters optimization

In order to obtain good broadband circular polarization performance, a series of parameter optimizations are processed on the proposed Ant. 4 structure. By changing the different structural parameters separately, the influences of the parameters on the antenna's performance are investigated. The optimization on the geometric parameters of the antenna are conducted in this way. In particular, the investigations on the influences of

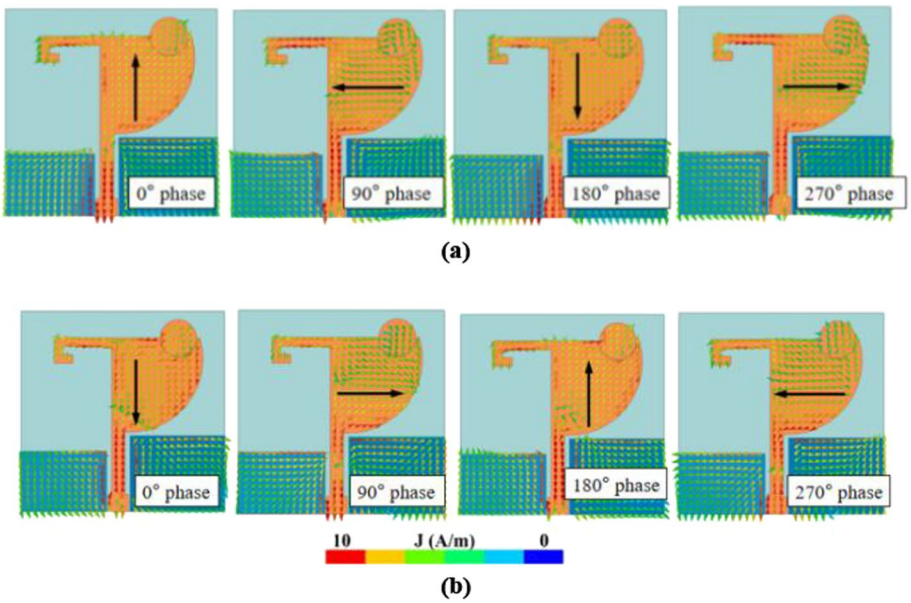

Fig. 4 Distributions of surface currents on the proposed antennas at **a** 6.5. **b** 8.5 GHz

the key parameters, including the length l_q of the monopole, the length l_1 of the folded microstrip stub line, the radius r of the circular patch, and the length m of the left ground, are compared and studied. Their effects on the antenna impedance bandwidth and AR bandwidth are analysed in the following part.

Figure 5 shows the influence of the radius l_q of the quarter-circle radiating patch on the antenna performance. The relationship of the 10-dB impedance bandwidth is shown in Fig. 5a, while the 3-dB ratio bandwidth of the antenna is shown in Fig. 5b. With the radius l_q varied from 11.05 mm to 11.35 mm, the impedance bandwidth is increased accordingly. The performance of the 3-dB AR bandwidth shows the same tendency. The overlapping frequency bands of the impedance and the AR are increased. At the same time, as the radius increasing from 11.25 to 11.35 mm, the AR value is greater than 3-dB when the working frequency is greater than 7.5 GHz. The optimized radius l_q is determined to be 11.25 mm. Since the monopole resonant frequency is determined by the monopole length, the monopole length shows great influence on the reflection coefficient and axial ratio characteristics of the antenna.

Figure 6 shows the effects of the length l_1 of one side of the folded microstrip stub line on the antenna reflection coefficient and the AR value. It can be seen from Fig. 6a that

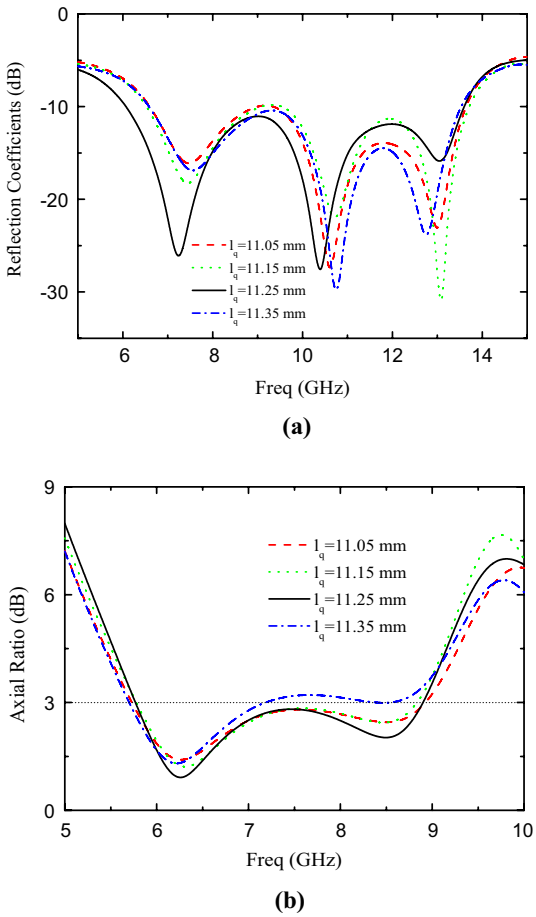

Fig. 5 The effect of different l_q on the performance of the proposed antenna. **a** Reflection coefficients at different frequencies with different l_q values. **b** AR at different frequencies with different l_q values

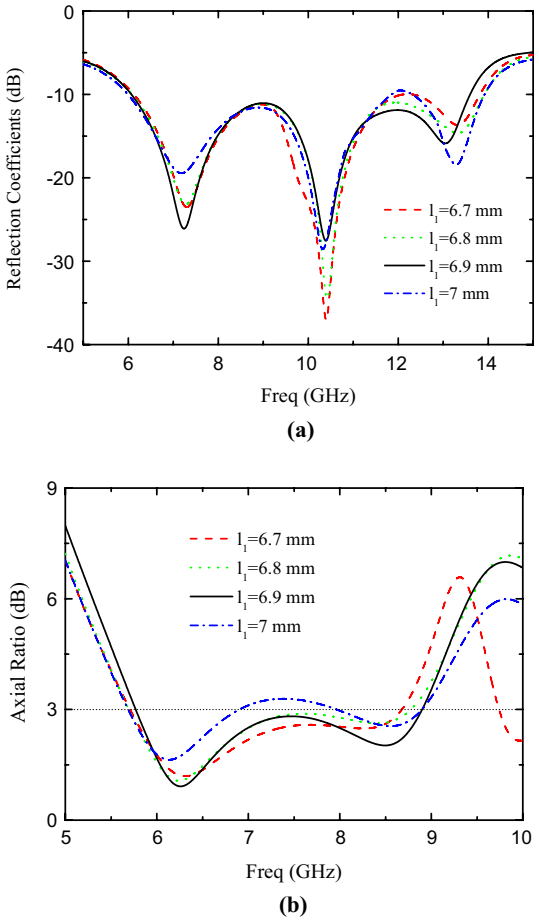

Fig. 6 Effects of different l_1 on the performance of the proposed antenna. **a** Reflection coefficients. **b** AR

the length of the L-shaped stub line has significant effect on the impedance matching of the antenna at the high frequency band. With the decreasing of the length l_1, the reflection characteristics of the high frequency band become worse. The current distribution on the microstrip stub line is significantly affected by the length of l_1. When l_1 is greater than 6.9 mm, the AR value is increased, while the 3-dB AR bandwidth is decreased. When l_1 is fixed to be 6.9 mm, the AR bandwidth is the largest, as shown in Fig. 6b.

Figure 7 shows the influences of the radius r of the coupled circular patch on the AR characteristics. If the radius r is decreased from 2 to 1.8 mm, the AR is increased, while the 3-dB AR bandwidth is decreased. The AR begins to be deteriorated when r is increased to be 2.1 mm. Therefore, r is selected to be 2 mm to achieve wider AR bandwidth.

The length m of the ground microstrip on the left side of the feeder is another important parameter that affects the AR performance of the antenna. Figure 8 shows the AR curves with different m values. The length m shows significant impact on AR performance at 8.5 GHz, while with less impact on AR at low frequencies. When m is smaller or larger than 7.2 mm, the AR value increases sharply around 8.5 GHz, while the AR bandwidth decreases. Finally the optimal length of m is chosen to be 7.2 mm in the design.

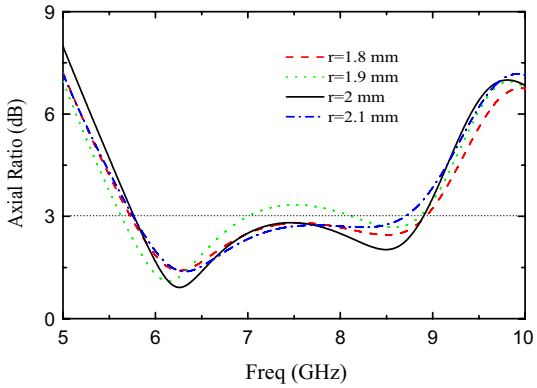

Fig. 7 Influence of radius r of coupled circular patch on antenna AR performance

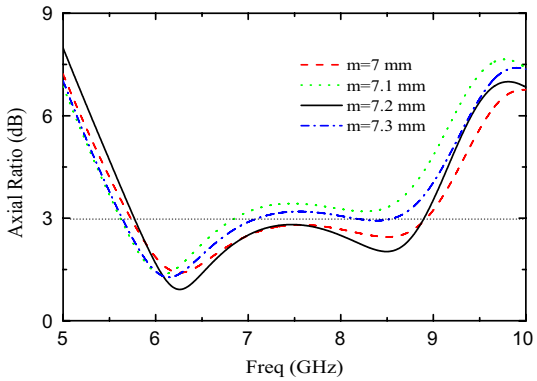

Fig. 8 Influence of antenna ground plate length m on antenna AR performance

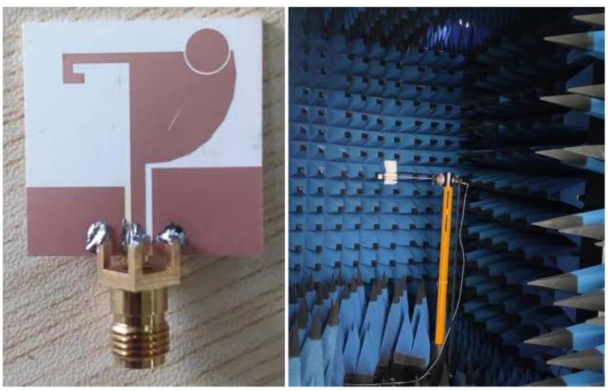

Fig. 9 Fabrication and measurement of the proposed antenna. **a** The photo of the fabricated CPW antenna. **b** The testbed of the measured antenna in the darkroom

3.2 Measurement results

Figure 9 shows the test setup of this circularly polarized antenna in the microwave anechoic chamber. The tested antenna is installed on the 2D turntable. The reference

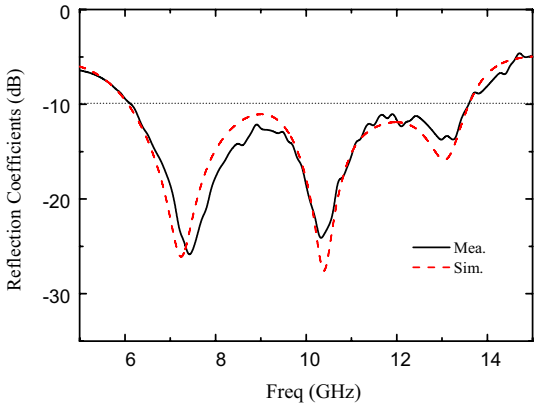

Fig. 10 Measurement curves of the reflection coefficient of the proposed UWB circularly polarized antenna. The simulation results are also included for the comparison

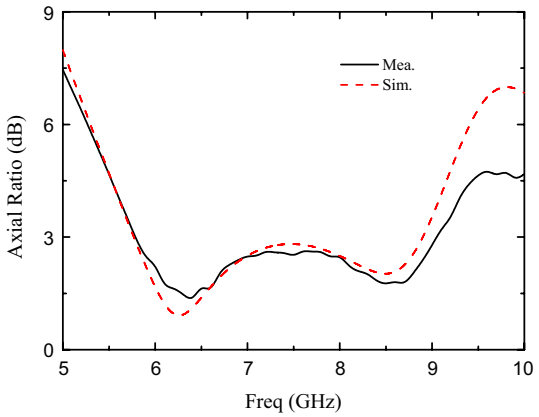

Fig. 11 The measurement curves of AR characteristics of the proposed UWB circularly polarized antenna. The simulation results are also included for the comparison

antenna is a standard horn antenna (LB-8180-NF). Two reference antennas are used in the test, acting as the receiving antenna and the transmitting antenna, which are connected with the two ports of the vector network analyzer (E8362B), respectively. The distance between the two reference antennas is set to be 5 m. The antenna gain is obtained by the comparison method, in which the reference antenna is taken as the compared target. The radiation efficiency is obtained by integrating the antenna gain modes on the whole sphere. The measurement is conducted in the far field of the anechoic chamber.

Figure 10 shows the measurement results of the antenna reflection coefficient. The frequency range is varied from 6.05 to 13.62 GHz with the reflection coefficient less than -10 dB. The impedance bandwidth achieves 7.57 GHz (76.9%), which is basically consistent with the simulation results. The measured and simulated AR curves are shown in Fig. 11. The measured AR value is less than 3 dB, and the bandwidth is between 5.8 and 9.06 GHz. The 3-dB AR bandwidth of the overlapped part with the impedance bandwidth is 3.01 GHz (6.05 GHz-9.06 GHz, 39.8%). As shown in Figs. 10 and 11, there are some discrepancies between the measured results and the simulated ones. It can be seen that the measured axial ratio and return flow loss are fluctuating

during the measurement. The error mainly comes from the fabrication process and the measurement error.

The gain and radiation efficiency measurement curves of the antenna are shown in Fig. 12. With the 3-dB AR bandwidth in the range of 6.05–9.06 GHz, the gain is between 0.46 and 3.28 dBi. The proposed antenna shows good radiation efficiency. The average radiation efficiency measured in the operating frequency band is 88.9%. The radiation efficiency of the antenna is affected by both the structure of the antenna and the test environment. Figure 13 shows the radiation patterns of the xoz plane and yoz plane of the CP antenna when the operating frequencies are 6.3 GHz, 7.5 GHz, and 8.5 GHz, respectively.

Table 2 shows the comparison of the proposed antenna with the other published works. As shown in Table 2, the UWB CP antenna proposed in the paper exhibits the widest operating bandwidth, and the highest gain, with competitive size. The antenna proposed in [17] has a simple structure, but the AR bandwidth is narrow. Ref. [18] uses dual port feeding to achieve dual circular polarization mode, while the antenna in the paper only needs one port to achieve right/left circular polarization in the $\pm z$ axis direction at the same time. The antenna size of Ref. [19] is large, so it is not easy to be conformal with the equipment. The axial ratio bandwidth of Ref. [20] antenna is narrow. Both Ref. [31] and [32] have achieved high gain, but the axial ratio bandwidth is narrow, the structure is complex, and the size is large. The CPW feeding mode is adopted in Ref. [33], and the antenna structure is simple, but the antenna gain is smaller than that proposed in the paper. Ref. [34] has a high profile, which is not conducive to conformal conformation with other devices.

Figure 13 shows the RHCP & LHCP radiation patterns measured in the xoz and yoz planes, corresponding to the different frequencies, including 6.3 GHz (as shown in Fig. 13(b)), 7.5 GHz (Fig. 13(b)) and 8.5 GHz (Fig. 13(c)). It can be seen that the antenna radiates a bidirectional wave with the opposite circular polarization. The RHCP is realized for $z > 0$, while LHCP for $z < 0$.

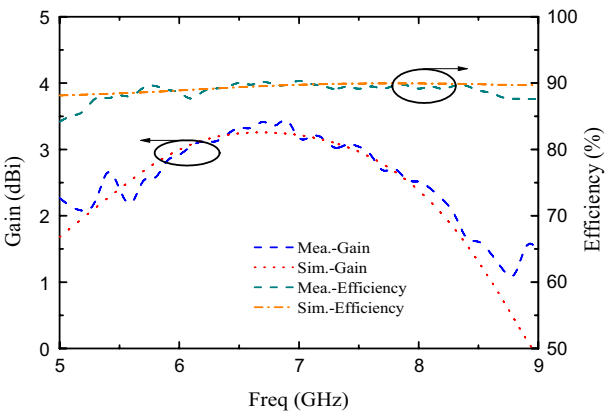

Fig. 12 Measured curves of the proposed UWB circularly polarized antenna gain. The simulation results are also included for the comparison

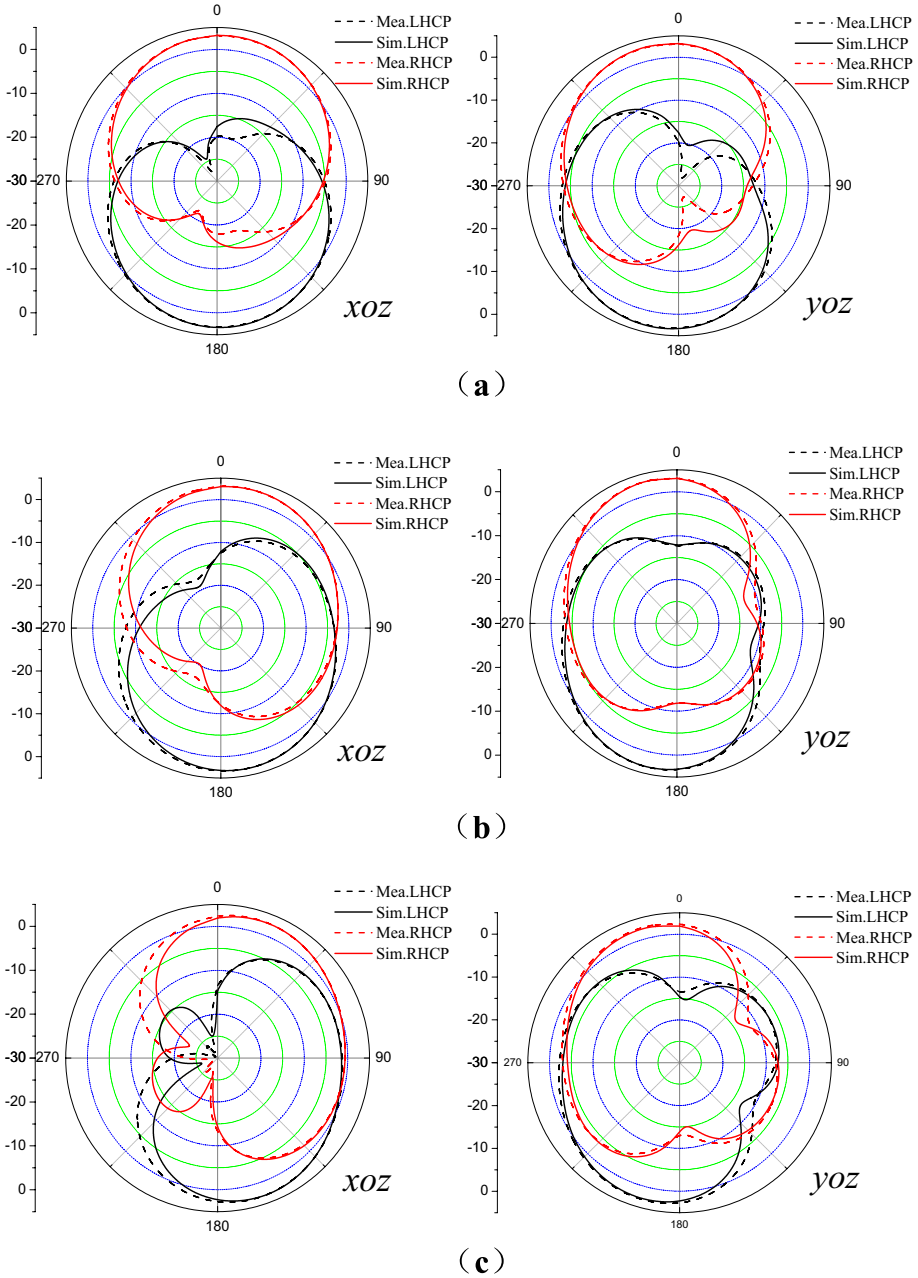

Fig. 13 RHCP & LHCP radiation patterns measured in the xoz and yoz planes. **a** 6.3 GHz. **b** 7.5 GHz. **c** 8.5 GHz. The simulation results are also included for the comparison

4 Conclusions

Circularly polarized antennas play a vital role in wireless communication systems and are widely used in devices such as radar, satellites, televisions, and drones. The CPW single-feed technology proposed in the paper, can achieve broadband circular polarization by the exciting quarter-circular radiating monopole patches, the folded microstrip stub lines, and the coupled circular patches in the structure. The single-fed circularly polarized antenna is simple in structure, with low-cost, which can be used in mobile equipment terminals.

Table 2 Comparison with the published CP antennas

References	IBW (S11 < −10 dB) (GHz)	3-dB ARBW (GHz)	Antenna size (λ_0^3)	Peak Gain (dBi)	Type
[7]	3.48–7.83	4.58–7.23	0.5 × 0.5 × 0.02	1.9	CPW
[17]	5.67–5.86	5.67–5.86	1.61 × 0.38 × 0.019	0.48	CPW
[18]	1.9–14.3	1.9–5.9	0.64 × 0.64 × 0.01	4	CPW
[19]	3.1–17.5	5.96–10.58	0.8 × 0.66 × 0.02	5	CPW
[20]	2.76–14.82	4.27–6.13	0.41 × 0.41 × 0.01	3	CPW
[31]	4.42–6.55	5.20–6.00	1.4 × 1.4 × 0.057	4.4	CPW
[32]	4.73–9.00	4.80–7.40	0.8 × 0.8 × 0.3	8.6	Microstrip
[33]	4.20–9.05	5.40–8.65	0.625 × 0.625 × 0.02	3.1	CPW
[34]	5.7–6.75	5.19–6.78	1.35 × 1.35 × 0.03	3.5	Coaxial
This work	6.05–13.62	6.05–9.06	0.61 × 0.62 × 0.02	3.28	CPW

IBW impedance bandwidth, *ARBW* Axial ratio bandwidth

The designed CPW single-feed UWB circularly polarized antenna has 10-dB impedance bandwidth of 76.9% and 3-dB axial ratio bandwidth of 39.8%. In the operating band, the measured gain is greater than 3-dBi and the antenna can generate right/left hand circularly polarized waves in the direction of ± z axis. It has wide application prospects due to its low profile, easy confomity with other communication devices and wider axial ratio bandwidth.

Abbreviations

CP	Circularly polarized
CPW	Coplanar waveguide
AR	Axial ratio
IoT	Internet of Things
RFID	Radio-frequency identification
CA	Cubic antenna
UWB	Ultra-wideband
PQMD	Quasi-magnetic dipole
HFSS	High Frequency Structure Simulator

Author contributions'

ZM provided critical feedback, contributed to the research of this project. JC conceived the study and the experiments. ZM and YJ carried out the experiments and data analysis. All authors discussed the results and participated in drafting and revising the manuscript.

Funding

This research was funded by the Fujian Natural Science Foundation Project, Grant Number 2022J01823.

Availability of data and materials

Data sharing not applicable to this article as no datasets were generated or analysed during the current study.

Declarations

Competing Interests

The authors declare that they have no competing interests.

Received: 23 December 2022 Accepted: 5 March 2023
Published online: 20 March 2023

References

1. J.S. Row, Design of square-ring microstrip antenna for circular polarisation. Electron Lett. **40**, 93–95 (2004). https://doi.org/10.1049/el:20040094
2. Y.F. Lin, H.M. Chen, S.C. Lin, A new coupling mechanism for circularly polarized annular-ring patch antenna. IEEE Trans. Antennas Propag. **56**, 11–16 (2008). https://doi.org/10.1109/TAP.2007.912961

3. K.L. Wong, C.C. Huang, W.S. Chen, Printed ring slot antenna for circular polarization. IEEE Trans. Antennas Propag. **50**, 75–77 (2002). https://doi.org/10.1109/8.992564
4. Y.M. Cai, K. Li, Y.Z. Yin, W. Hu, Broadband circularly polarized printed antenna with branched microstrip feed. IEEE Antennas Wirel. Propag. Lett. **13**, 674–677 (2014). https://doi.org/10.1109/LAWP.2014.2314317
5. C.Y. Huang, K.L. Wong, Coplanar waveguide-fed circularly polarized microstrip antenna. IEEE Trans. Antennas Propag. **48**, 328–329 (2000). https://doi.org/10.1109/8.833083
6. J.W. Wu, J.Y. Ke, C.J. Wang, Microstrip-fed broadband circularly polarized monopole antenna. Microw. Antennas Propag. **4**, 518–525 (2010). https://doi.org/10.1049/iet-map.2008.0400
7. L. Zhang, Y.C. Jiao, Y. Dong, B. Chen, Z.B. Weng, CPW-fed broadband circularly polarized planar monopole antenna with improved ground-plane structure. IEEE Trans. Antennas Propag. **61**, 4824–4828 (2013). https://doi.org/10.1109/TAP.2013.2267719
8. T. Kumar, A.R. Harish, Broadband circularly polarized printed slot-monopole antenna. IEEE Antennas Wireless Propag. Lett. **12**, 1531–1534 (2013). https://doi.org/10.1109/LAWP.2013.2291436
9. R.C. Han, S.S. Zhong, Broadband circularly-polarized chifre-shaped monopole antenna with asymmetric feed. Electron. Lett. **52**, 256–258 (2016). https://doi.org/10.1049/el.2015.3319
10. B. Hu, Nasimuddin, Z. Shen, Moon-shaped printed monopole antenna for wideband circularly polarized radiation. Proc. Int. Conf.. *IEEE-APS Top. Conf. Antennas Propag. Wireless Commun* (2013). doi:https://doi.org/10.1109/APWC.2013.6624912.
11. C.J. Wang, Y.C. Lin, New CPW-fed monopole antennas with both linear and circular polarisation. IEEE Microw. Antennas Propag. **2**, 466–472 (2008). https://doi.org/10.1049/iet-map:20070145
12. C.J. Wang, C.H. Chen, CPW-fed stair-shaped slot antennas with circular polarization. IEEE Trans. Antennas Propag. **57**, 2483–2486 (2009). https://doi.org/10.1109/TAP.2009.2024586
13. S.W. Zhou, P.H. Li, Y. Wang, W.H. Feng, Z.Q. Liu, A CPW-fed broadband circularly polarized regular-hexagonal slot antenna with L-shape monopole. IEEE Antennas Wireless Propag. Lett. **10**, 1182–1185 (2011). https://doi.org/10.1109/LAWP.2011.2172570
14. V. Kaim, B.K. Kanaujia, K. Rambabu, Quadrilateral spatial diversity circularly polarized MIMO cubic implantable antenna system for biotelemetry. IEEE Trans. Antennas Propag. **69**, 1260–1272 (2020). https://doi.org/10.1109/TAP.2020.3016483
15. A. Gharaati, M.S. Ghaffarian, H. Saghlatoon, M. Behdani, R. Mirzavand, A low-profile wideband circularly polarized CPW slot antenna. AEU-Int. J. Electron. Commun. (2021). https://doi.org/10.1016/j.aeue.2020.153534
16. R. Xu, Z. Shen, S. Gao, Compact-size ultra-wideband circularly polarized antenna with stable gain and radiation pattern. IEEE Trans. Antennas Propag. **70**, 943–952 (2021). https://doi.org/10.1109/TAP.2021.3111316
17. J. Yang, X. Li, L. Yang, A novel design of CPW feed planar omnidirectional circularly polarized antenna. Int. J. Antennas Propag. **2**, 1–7 (2021). https://doi.org/10.1155/2021/6695966
18. Z. Li, Zhu. X, Y. C, CPW-fed ultra-wideband slot antenna with broadband dual circular polarization. *AEU-International Journal of Electronics and Communications* (2019). https://doi.org/10.1016/j.aeue.2018.11.018.
19. C. Prashant, Kumar. As, Compact ultra-wideband circularly polarized CPW-fed monopole antenna. *AEU-International Journal of Electronics and Communications* (2019). https://doi.org/10.1016/j.aeue.2019.05.025.
20. S. M, R. V, K. S, Z. Amiri, B. Virdee, Miniaturised ultra-wideband circularly polarised antenna with modified ground plane. *Electron. Lett.* 50, 1786–1788(2014). https://doi.org/10.1049/el.2014.3278.
21. S.R. Best, A discussion on the significance of geometry in determining the resonant behavior of fractal and other non-Euclidean wire antennas. IEEE Antennas Propag. Mag. **45**, 9–28 (2003). https://doi.org/10.1109/MAP.2003.1232160
22. E. Guariglia, Entropy and fractal antennas. Entropy **18**, 84 (2016). https://doi.org/10.3390/e18030084
23. S.R. Best, Operating band comparison of the perturbed Sierpinski and modified Parany gasket antennas. IEEE Antennas Wireless Propag. Lett. **1**, 35–38 (2002). https://doi.org/10.1109/LAWP.2002.802584
24. E. Guariglia, Harmonic Sierpinski gasket and applications. Entropy **20**, 714 (2018). https://doi.org/10.3390/e20090714
25. R.G. Hohlfeld, N. Cohen, Self-similarity and the geometric requirements for frequency independence in antennae. Fractals **7**, 79–84 (1999). https://doi.org/10.1142/S0218348X99000098
26. D.H. Werner, S. Ganguly, An overview of fractal antenna engineering research. IEEE Antennas Propag. Mag. **45**, 38–57 (2003). https://doi.org/10.1109/MAP.2003.1189650
27. E. Guariglia, S. Silvestrov, *Fractional-Wavelet Analysis of Positive definite Distributions and Wavelets on D'(C)* (International Publishing, Springer, 2016), pp.337–353
28. E. Guariglia, R.C. Guido. Chebyshev Wavelet Analysis. *J. Funct. Spaces.* 2022, (2022). doi:https://doi.org/10.1155/2022/5542054.
29. M.D. Deshpande, M.C. Bailey, Analysis of stub loaded microstrip patch antennas. IEEE Antennas Propag. Soc. Int. Symp. (1997). https://doi.org/10.1109/APS.1997.631535
30. J.A Ansari, A. Singh, A. Mishra, Analysis of L-strip fed gap coupled compact semi-circular disk patch antenna. *International Conference on Multimedia, Signal Processing and Communication Technologies*, IEEE, Aligarh, India (2011). doi:https://doi.org/10.1109/MSPCT.2011.6150469.
31. C. Zhao, C.F. Wang, Characteristic mode design of wide band circularly polarized patch antenna consisting of H-shaped unit cells. IEEE Access. **6**, 25292–25299 (2018). https://doi.org/10.1109/ACCESS.2018.2828878
32. W. Yang, J. Zhou, Wideband circularly polarized cavity-backed aperture antenna with a parasitic square patch. IEEE Antennas Wirel. Propag. Lett. **13**, 197–200 (2014). https://doi.org/10.1109/LAWP.2014.2298252
33. U. Ullah, K. Slawomir, Enhanced axial-ratio bandwidth single-point-fed CP antenna using slot structure modification. IEEE Int. Sympos. Antennas Propag. USNC-URSI Radio Sci. Meet. (2019). https://doi.org/10.1109/APUSNCURSINRSM.2019.8889026
34. W. He, Z. Long, S.W. Wong, A wideband circularly polarized antenna with conical-beam radiation. *IEEE International Conference on RFID Technology and Applications (RFID-TA)* (2019). doi:https://doi.org/10.1109/RFID-TA.2019.8892105.

Publisher's Note